ADVANCED MATERIALS

Supporting Information

for *Adv. Mater.*, DOI: 10.1002/adma.201203374

Bioinspired Surfaces with Dynamic Topography for Active Control of Biofouling

Phanindhar Shivapooja, Qiming Wang, Beatriz Orihuela, Daniel Rittschof, Gabriel P. López, and Xuanhe Zhao**

Submitted to ADVANCED MATERIALS

Supporting Information

Bioinspired Surfaces with Dynamic Topography for Active Control of Biofouling

Phanindhar Shivapooja[†], *Qiming Wang*[†], *Beatriz Orihuela*, *Daniel Rittschof*, and *Gabriel P. López**, *Xuanhe Zhao**

[†] These authors contributed equally to this work.
*Email: gabriel.lopez@duke.edu; xuanhe.zhao@duke.edu

S1. Effect of shear flow alone on the detachment of biofilms

Biofilms formed on Sylgard 184 surfaces were subjected to a continuous flow of artificial sea water at 0.5 mL/min for 10 minutes as shown in **Figure S1a**. Analysis of the biofilm surfaces before and after flow did not show any significant detachment of the adhered biofilms as shown in **Figure S1b and c**. Thus, the flow was only able to remove the detached biofilm upon electro-actuation (**Figure 1**).

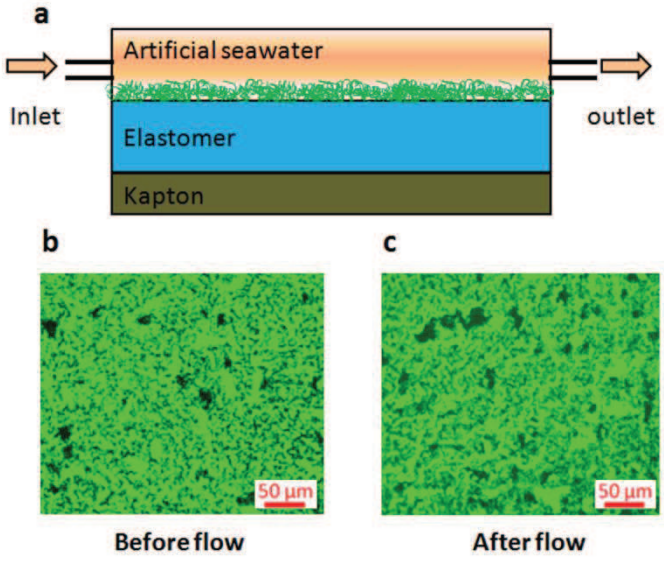

Figure S1. **Effect of the shear flow on detachment of biofilms.** (a) Schematic showing the flow on the *Cobetia marina* biofilm grown on Sylgard 184 for 6 days. Fluorescence images of the stained biofilm captured using 10 x objective (b) before flow and (c) after flow.

S2. Characterization of surface strain

The surface strain due to electro-actuation was characterized using markers imprinted on the surface. The fabrication procedure for the surface with markers is shown in **Figure S2a**. In brief, the markers were fabricated by casting a 50 μm thick Sylgard 184 film on a silicon mold with pillars arranged in a square lattice generated with photolithography. The feature size of the pillars on the mold is represented in **Figure S2a**. The distance between two adjacent pillars (5 μm) is much smaller than the thickness (50 μm) of the Sylgard 184 film. Therefore, the markers have negligible effect on the deformation of the Sylgard 184 film. Images (shown in **Figure S2b**) of the Sylgard 184 surface at flat and deformed states were captured by a microscope (Nikon, Japan). The initial (X_J) and deformed coordinates (x_i) were measured with an image processing software (ImageJ, NIH, USA) and the deformation gradient $F_{iJ} = \partial x_i / \partial X_J$ was computed using finite element analysis [31]. The Green strain was then calculated as $E = \left(F^T F - I\right)/2$, where I denotes the Kronecker delta tensor. The maximum principal Green strain was computed and plotted in Figure 1b.

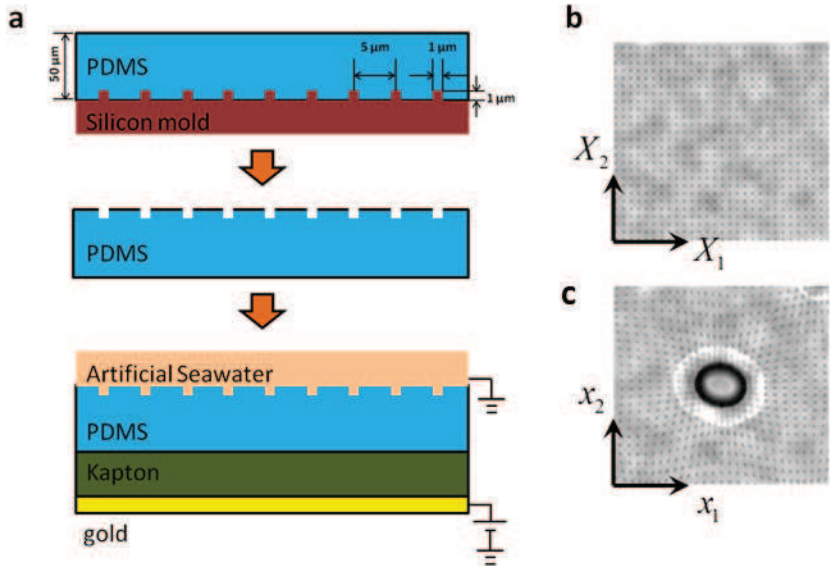

Figure S2. Surface deformation due to electro-actuation. (a) Schematic illustration of process for fabrication of the Sylgard 184 surface with markers. Phase contrast optical microscopy images of the Sylgard 184 surface in the undeformed, flat state (b) and the deformed, "cratered" state (c).

S3. Biofilm morphology on deformed substrate

Biofilms of *Cobetia marina* were grown on rectangular Ecoflex surfaces for six days and stained (see Methods). The stained biofilm gave a uniform coverage over most area of the Ecoflex surface as shown in **Figure S3a**. The Ecoflex substrate with the stained biofilm was then clamped on two opposing edges and slowly stretched in a uniaxial direction to 20% strain. The substrate was held in the stretched state and observed under the microscope to examine the effect of surface deformation on biofilm morphology. As shown in **Figure S3b**, the biofilms on the deformed substrate maintained its integrity over a length scale much larger than the thickness of the biofilms (i.e. 30 µm- 80 µm). Therefore, the detachment of the biofilm can be analyzed as a debonding process of a film from substrate.

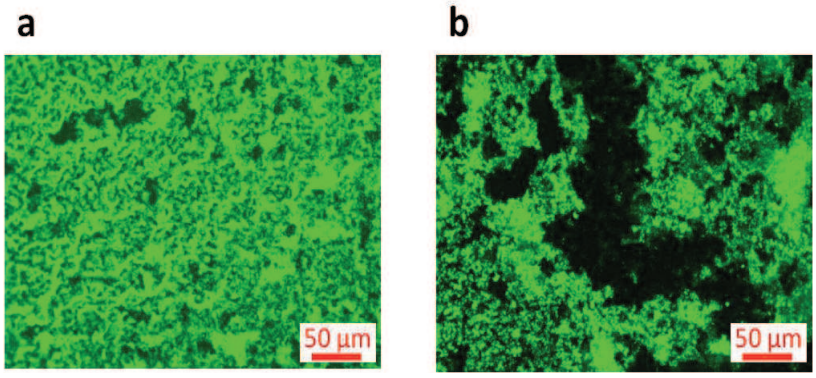

Figure S3. Fluorescence microscopy images of *Cobetia marina* biofilm surface before stretching (a) and after stretching to 20% strain (b).

S4. Energy release rate for debonding of barnacles.

The system of a row of barnacles on an elastomer film (**Figure 3c**) was simplified as a 2D plane-strain model as shown in **Figure S4a**. The Ecoflex film was modeled as a Neo-Hookean material with shear modulus μ_s and was assumed to be infinitely thick. The barnacle was modeled as a rigid body. The bonding length between the barnacle and the polymer substrate is denoted as L. The energy release rate G was computed by a commercial finite element package ABAQUS 6.10.1 (SIMULIA, USA). As shown in **Figure S4b**, the normalized energy release rate $G/(\mu_s L)$ increases with the applied strain e and the normalized contact length L/S, where S is the width of the polymer film. If the applied strain is small (e< 10%), the energy release rate can be analytically expressed as[32]

$$G = \frac{1}{2}\mu_s L\left[e^2 \tan\left(\frac{\pi L}{2S}\right)\left(\frac{S}{L}\right)\right] \qquad \text{(S1)}$$

In addition, if S is much larger than L, Equation (S1) further reduces to $G = \pi\mu_s L e^2/4$. From **Figure S4b**, it can be seen that the numerically calculated G at low values of e and L/S matches consistently with the analytical solution.

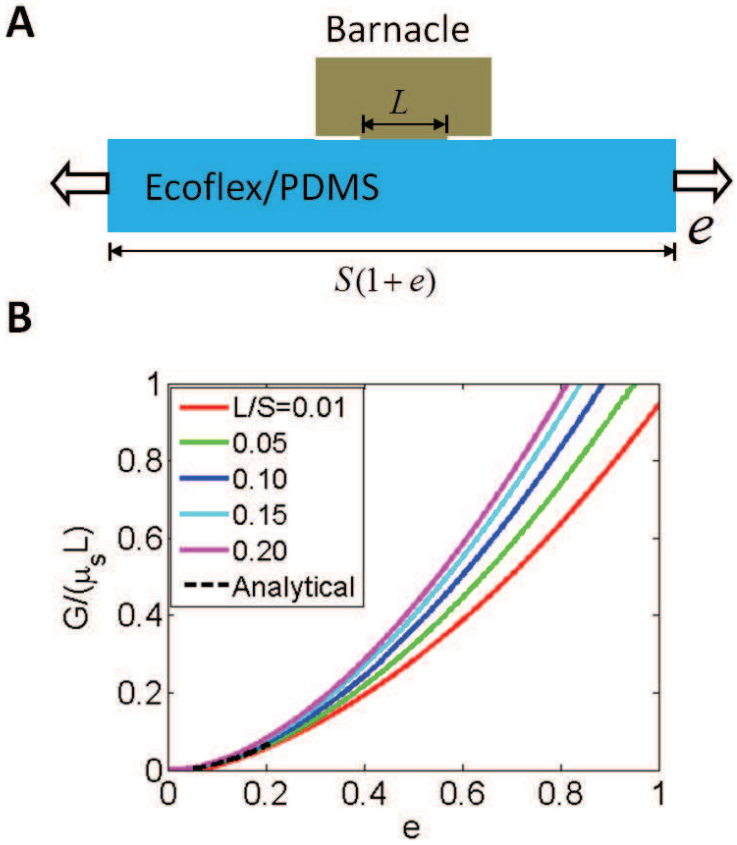

Figure S4. Normalized energy release rate for debonding of barnacle from the substrate. (a) Schematic for the elastomer-barnacle system under uniaxial stretching. (b) The relation between the normalized energy release rate with applied strain e and the ratio L/S.

S5. Biofilm thickness measurements

As shown in **Figure S5**, the thickness of the biofilm formed on the surface was measured using an inverted confocal microscope (Zeiss LSM 510) equipped with an argon ion laser operating at an excitation wavelength of 488 nm. For imaging, the biofilm was stained using SYTO 13 (see Methods). Using a 40X objective, a series of images were collected across the depth of the biofilm using the Z-stack software module provided by Zeiss. The start and end points for Z-stack imaging were determined by doing a fast XY scan while focusing on and out of the specimen surface; the images were automatically captured at each z-axis depth interval of 3 μm.

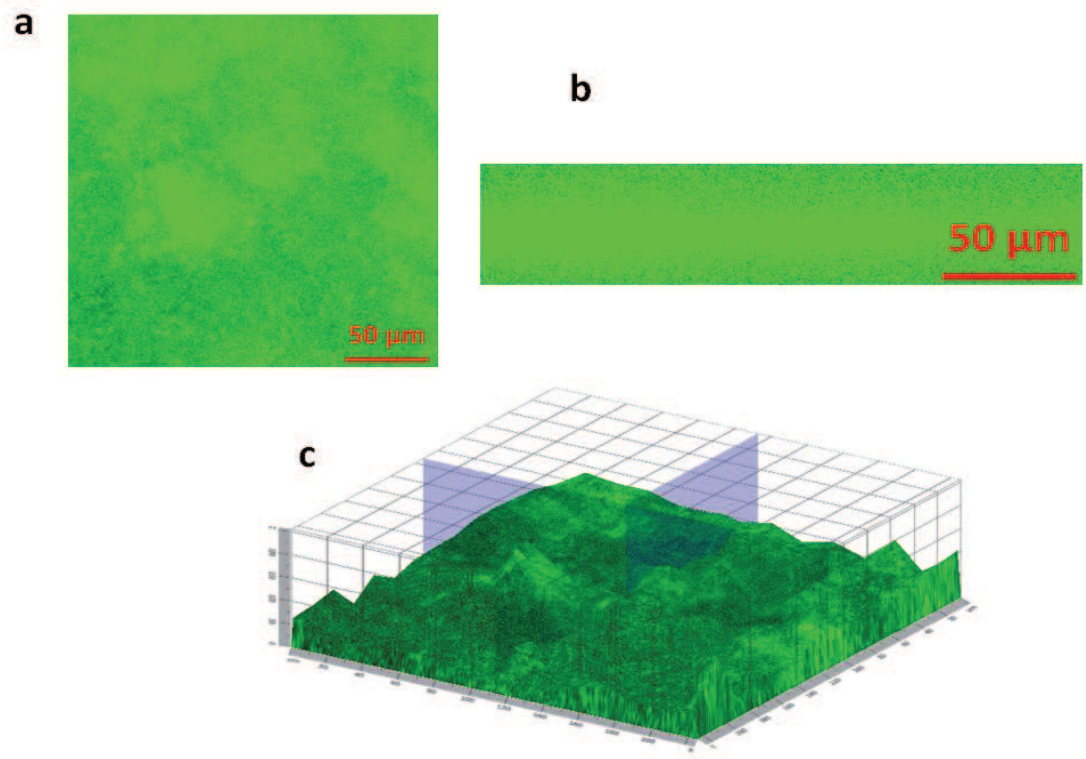

Figure S5. Confocal images of the Cobetia marina biofilm grown on Ecoflex for 4-days. (a) Z-stack image of *Cobetia marina* biofilm surface as seen from the top, (b) the cross-sectional view of the biofilm and (c) the 3-D reconstruction image of the biofilm.

S6. Process for fabrication of pressure-actuation prototype

As shown in **Figure S6**, a plastic prototype fabricated by a 3D printer (Stratasys, USA) was used as a mold to cast a patterned Ecoflex network. The network (**Figure S6b**) was then placed over an uncured Ecoflex film (~200 µm) spin-coated on a glass slide. After curing, the patterned Ecoflex network was firmly bonded to the glass slide to form enclosed air channels. Each air channel was covered by a long Ecoflex strips with thickness of ~1mm. Small holes were punched on two opposite walls of the network: one connected to a rubber tubing for air inlet and the other to a digital pressure transducer (Tachikara Inc.). As air pressure in the channels increases, the thin Ecoflex strip above the air channel buckles upward generating surface deformation.

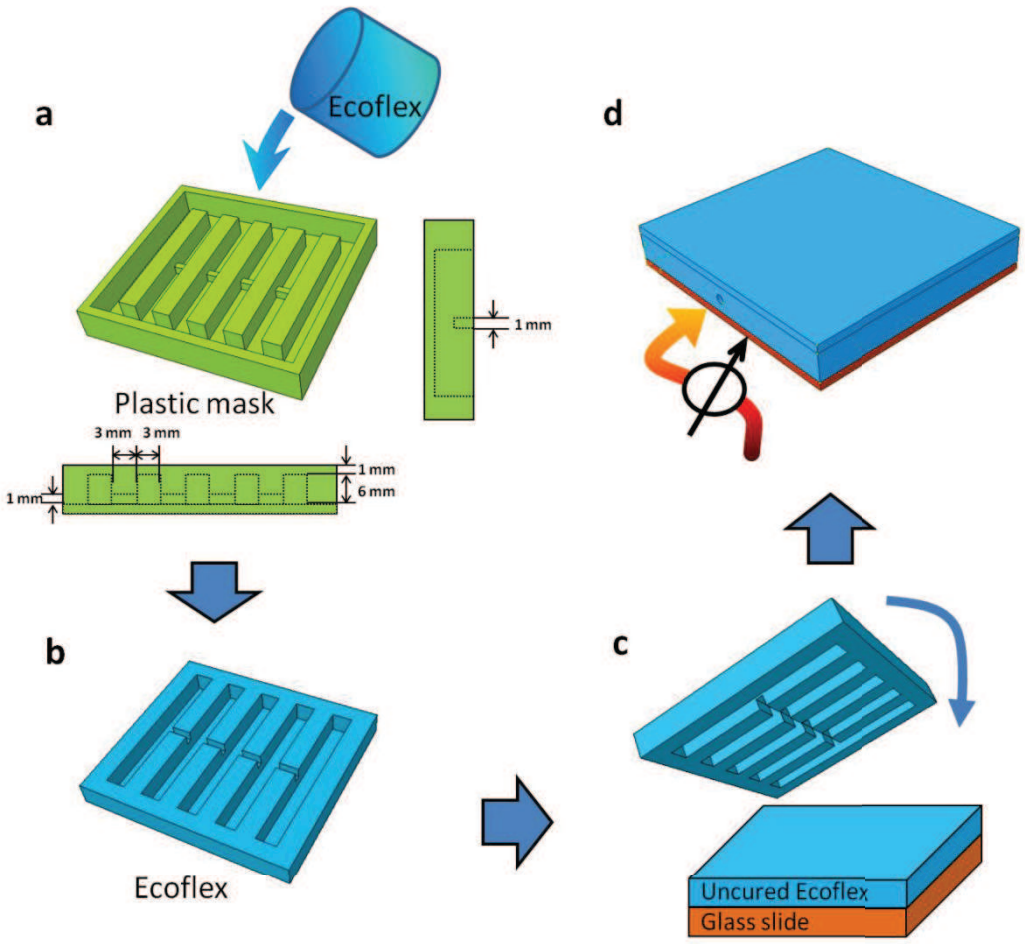

Figure S6. Fabrication of dynamic surfaces actuated by pressurized air. (a) A plastic prototype fabricated by a 3D printer was used as a mold to cast a patterned Ecoflex network. (b) Patterned Ecoflex with air-pass channels inside. (c) The patterned Ecoflex with air-pass channels inside was adhered on a glass slide with uncured Ecoflex. (d) After curing, the patterned Ecoflex with embedded air channels was firmly bonded to a glass slide.

S7. Pressure vs. strain for dynamic surfaces actuated by pressurized air

The pressure-controlled buckling of the Ecoflex strip above the air channel network was modeled as shown in **Figure S7a** [33]. A 2D plane-strain model was constructed to account for the deformation of the long Ecoflex strip. The Ecoflex strip clamped at two ends was subjected to a uniform pressure P, buckling out as an arc with radius R. We denote the initial

and blistered length as $2L$ and $2l$, and initial and blistered thickness of the film as H and h. As illustrated in **Figure S7a**, force balance gives

$$PR = \sigma_\theta h \tag{S2}$$

where σ_θ is the membrane stress. The two principal stretches in the film are

$$\lambda_\theta = \frac{l}{L} = \frac{\theta}{\sin\theta}, \quad \lambda_r = \frac{h}{H} = \frac{1}{\lambda_\theta} \tag{S3}$$

where 2θ is the angle of the arc as show in **Figure S7a**. The Ecoflex film obeys the Neo-Hookean model, i.e.

$$\sigma_\theta = \mu\lambda_\theta^2 - P_0, \;\; \sigma_r = \mu\lambda_r^2 - P_0 \tag{S4}$$

where P_0 is the hydrostatic pressure to ensure the imcompressibility of the elastomer. Given that the radial stress $\sigma_r \approx 0$, Equation (S4) gives

$$\sigma_\theta = \mu\left(\lambda_\theta^2 - \lambda_r^2\right) \tag{S5}$$

Combining Equations. (S2, S3, and S5), we can calculate the relation between the applied pressure P and the surface strain of the Ecoflex film $e = \lambda_\theta - 1$. The theoretical results consistently match with the experimental data (**Figure S7b**).

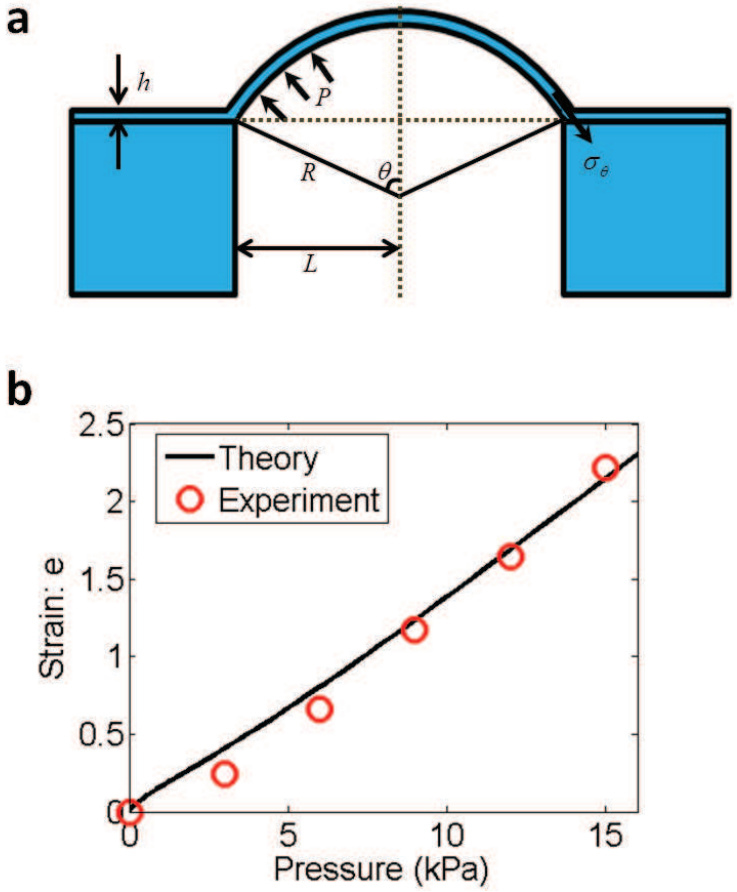

Figure S7. Pressure vs. strain for dynamic surfaces actuated by air pressure. (a) 2D schematic for blistering of the Ecoflex surface due to air pressure. (b) Relation between the surface strain and the air pressure.

Additional References

31. Hughes, T. J. R. *The finite element method: linear static and dynamic finite element analysis*. Vol. 65 (Dover Publications, 2000).
32. Lu, N., Yoon, J. & Suo, Z. Delamination of stiff islands patterned on stretchable substrates. *International Journal of Materials Research* **98**, 717-722, doi:10.3139/146.101529 (2007).
33. Williams, J. Energy release rates for the peeling of flexible membranes and the analysis of blister tests. *International Journal of Fracture* **87**, 265-288 (1997).